

Article

# A Proposal to Evaluate Drought Characteristics Using Multiple Climate Models for Multiple Timescales

Nguyen Tien Thanh 

Department of Hydro-meteorological Modeling and Forecasting, Thuyloi University,  
175 Tay Son, Dong Da, Hanoi, Vietnam; thanhnt@tlu.edu.vn

Received: 23 August 2018; Accepted: 18 September 2018; Published: 20 September 2018



**Abstract:** This study presents a method to investigate meteorological drought characteristics using multiple climate models for multiple timescales under two representative concentration pathway (RCP) scenarios, RCP4.5 and RCP8.5, during 2021–2050. The methods of delta change factor, unequal weights, standardized precipitation index, Mann–Kendall and Sen’s slope are proposed and applied with the main purpose of reducing uncertainty in climate projections and detection of the projection trends in meteorological drought. Climate simulations of three regional climate models driven by four global climate models are used to estimate weights for each run on the basis of rank sum. The reliability is then assessed by comparing a weighted ensemble climate output with observations during 1989–2008. Timescales of 1, 3, 6, 9, 12, and 24 months are considered to calculate the standardized precipitation index, taking the Vu Gia–Thu Bon (VG–TB) as a pilot basin. The results show efficient precipitation simulations using unequal weights. In the same timescales, the occurrence of moderately wet events is smaller than that of moderately dry events under the RCP4.5 scenario during 2021–2050. Events classified as “extremely wet”, “extremely dry”, “very wet” and “severely dry” are expected to rarely occur under the RCP8.5 scenario.

**Keywords:** multiple climate models; standardized precipitation index (SPI); droughts; weights; Vu Gia–Thu Bon

## 1. Introduction

Drought is a natural hazard related to a deficiency of precipitation for an extended period that results in water shortage for some activities or for some economic sectors [1]. The meanings of “drought” depend on different perspectives of stakeholders from farmers to meteorologists [2]. Commonly, according to the studies of droughts [3–5], the concept of drought is clustered into four types consisting of meteorological, agricultural, hydrological and socioeconomic types. The Intergovernmental Panel on Climate Change (IPCC) Fourth Assessment Report [6] emphasizes that the world indeed has become more drought-prone during the past 25 years. Drought-affected areas will likely increase in frequency and severity, with implications for sustainable development (e.g., agriculture and forestry production or land degradation). Observed changes in characteristics of droughts (i.e., more intense and longer duration droughts) are widely documented for a variety of regional and ocean basin scales since the 1970s with the emphasis on tropics and subtropics [6]. In comparison to the Medieval Climate Anomaly (950–1250), more megadroughts appeared in monsoon Asia and wetter conditions became dominant in arid Central Asia and the South American monsoon region during the Little Ice Age (1450–1850) [7]. Over a global scale, it is observed that the intensity and/or duration of droughts likely increase in the Mediterranean and West Africa and decrease in central North America and north-west Australia [6]. Increased drying is directly linked to higher temperatures and decreased precipitation. It is noteworthy that the palaeoclimate records show that droughts prolonging with a scale of decades or longer have been very likely a repetitive feature of

the climate in several regions over the last 2000 years [6]. Overall, these studies show that several extreme droughts occurred in the last millennium. Moreover, it poses questions about the uncertainty of calculated results as well as how the projected droughts express their footprint on a local scale under different scenarios of climate change. There is an urgent need to find away to evaluate the droughts. This plays a central role in drought management strategies, and social responses to manage the risks and mitigate the drought impacts.

To evaluate the impacts of droughts on different fields (e.g., water shortages, concomitant shortages, crop growth), many drought indices have been developed and applied under timescales of short- or long-term. These indices widely vary from simple indices (e.g., percentage of normal precipitation) to sophisticated indices (e.g., Palmer drought severity index). Obviously, no drought index is suitable for all circumstances of a specific region. Some indices can be better suited than others for certain regional applications. Svoboda and Brian [8] showed some disadvantages of the standardized precipitation index (SPI) such as an assumption of distribution that can bias the results, particularly when examining short-duration events. In this study, however, the SPI index is still selected to calculate the drought-related components for numerous reasons: (1) the SPI index has been suggested and highlighted by the World Meteorological Organization [5], and nowadays many national meteorological services and drought monitoring centers use it (e.g., in the US [9]; in Europea [10]; and in Canada [11]); (2) the SPI is a powerful, flexible indicator based on robust underlying probability functions and it has high spatial coherence. Moreover, it is simple to calculate and needs only the required input parameter of precipitation. More importantly, Salehnia et al. [12] showed that eight precipitation-based drought indices, namely SPI, PNI (percent of normal index), DI (deciles index), EDI (effective drought index), CZI (China-Z index), MCZI (modified CZI), RAI (rainfall anomaly index), and ZSI (Z-score index) have similar trends; (3) lots of publications illustrated that precipitation data alone could explain most of the variability of drought (e.g., [13]). Furthermore, some indices (i.e., SPI, the standardized precipitation evapotranspiration index (SPEI: [14]), the Palmer drought severity index (PDSI: [15]); the self-calibrated PDSI [16] and the reconnaissance drought index (RDI: [17])) have been tested on a global scale by Spinoni et al. [18]. They showed that these indices have more difficulties than the SPI with possible error values such as a heat wave for a meteorological drought for the SPEI index or unrealistic extreme values for the RDI index; (4) the SPI index is designed to quantify the precipitation deficit for multiple timescales, reflecting the impact of drought on the water availability. For example, shorter SPI timescales (from 1 to 6 months) mainly indicate the drought index for agriculture practices like soil moisture conditions, whereas longer SPI timescales (from 12 to 48 months) indicate the drought index for hydrology like groundwater, streamflow and reservoir [5]. In this study, multiple timescales of the SPI index (1-, 3-, 6-, 9-, 12- and 24-month SPI) are considered using multiple climate models. The reason for this is that Vietnam is an agricultural country and has nearly 7000 reservoirs over the whole country. VG-TB has 6 reservoirs including the A Vuong, DakMi 4, Song Tranh 2, Song Bung 4, Song Bung 4A and Song Bung 5 reservoirs.

For climate projections, strictly speaking, the understanding of nature and its representation in climate models is mostly incomplete with sources of uncertainty (e.g., emissions of greenhouse gases, parameterization schemes of convective cloud and land surface, grid systems, map projections and climatic forcing factors). Thus, to be more reliable and accurate for climate projections, a combination of multiple climate models is widely applied. This pragmatic approach has received much attention over the availability of numerical weather and climate forecasts from institutions and centers of weather and climate research. To date, the metadata has been constructed such as the Ensemble-Based Predictions of Climate Changes and Their Impacts (ENSEMBLES) project [19] and phase 3, phase 5 and phase 6 of the Coupled Model Intercomparison Project (CMIP3, CMIP5 and CMIP6) using multiple climate models. Usually, the simplest method of constructing a multiple climate model is used with “equal weighting” in which weights equal  $1/M$ , where  $M$  is the number of models. In a more sophisticated manner, the approach of “unequal weighting” or “optimum weighting” is voted. Weigel et al. [1] discussed two ways of “equal weighting” and “unequal weighting”. The study showed that “equal weighting”

from multiple models perform better than the single models. Furthermore, the projection errors can be further eliminated by using “unequal weighting”. To get this, however, single model skills and relative contributions of the joint model error are required. More importantly, Timothy et al. [20] used a statistical test to define whether an ensemble of multi models with “unequal weighting” is significantly better than without “unequal weighting”. The study showed that a value for the relatively small global fraction is illustrated with the method of “unequal weighting”. Sanderson et al. [18] suggested a weighting scheme to eliminate some aspects of model codependency in the ensemble. Also, a weighting strategy for an ensemble of CMIP5 was presented by Sanderson et al. [21] in the fourth National Climate Assessment. In general, these studies use a distance metric of models to observations and the distance metric of a pair of models  $i$  and  $j$ , and a relationship to convert those into a weight. The equal weighting is, remarkably, often used to develop the global ensemble scenarios as a safer and more transparent way to combine models [1], but unequal weights can be better for some areas of the global [20]. In most cases of existing ensemble members, the application of any kind of weighting to ensemble variance is mostly discarded, but only considered the weighted mean [1,22,23]. This can ignore the intermodel relationships and unexpected values, as extreme weather variables can potentially be more sensitive to changes in the variance [24]. In addition, ensemble members typically come from the same model.

In the context of changing climate, studies in drought events at scales of region and basin are valuable for understanding their evolution and impacts on a wide range of fields (e.g., agriculture, socio-economic, environment and natural resources) that occur over certain areas. In this sense, the present study aims to evaluate the wet and drought events in the 21st century using multiple climate models for multiple timescales. The precipitation projections from multiple regional climate models driven by multiple global climate models are separately corrected using the method of delta change factor. In addition, an unequal weight method is proposed in the expectation of a better performance of multiple climate projections of precipitation at basin scale in Vietnam as a case study. Weights for each climate simulation are calculated on the basis of rank sum metric of each climate simulation. The rank sum is defined from statistical indices of each climate simulation in comparison with observation. In comparison with the existing methods mentioned above, this approach can measure not only the absolute performance of each model, but the performance compared with the other models in the ensemble with its ranks. The methods of the non-parametric Mann–Kendall (MK) test [25,26] and Sen’s slope [27] are then applied to detect the projection trends in meteorological drought for multiple timescales at a significance level of 0.05. The reason for this is that the MK test is widely applied [28–30] with advantages of a rank correlation without any request of a particular distribution of data and not affected by the data errors and outliers.

## 2. Materials and Methodology

### 2.1. Description of the Case Study Area: Vu Gia-Thu Bon Basin

A plot basin, Vu Gia-Thu Bon (VG-TB), is selected in this study. It is located in central Vietnam, elongating from  $16^{\circ}55'$  through  $14^{\circ}55'$  and from  $107^{\circ}15'$  through  $108^{\circ}24'$  and covers a total of area of approximately  $12,577 \text{ km}^2$ . The VG-TB basin is surrounded by two main provincial administrative territories Quang Nam and Da Nang. The basin is characterized by a steep topography and the altitude ranging from 0 m at the coast to 2567 m in elevation above sea level (m.a.s.l) in the west (Figure 1).

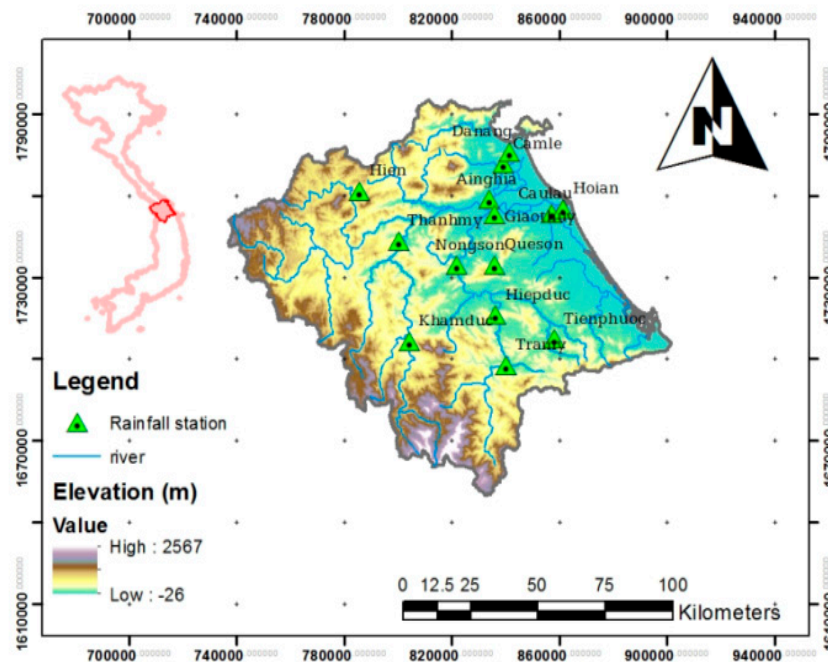


**Figure 1.** Network of hydro-meteorological stations at Vu Gia-Thu Bon (VG-TB) basin.

## 2.2. Data

### 2.2.1. Observational Data

The monthly precipitation records are obtained from the Vietnam HydroMeteorological Data Center of the Ministry of National Resources and Environment of Vietnam (MONRE). They are aggregated from the daily series of data. There are two national rain gauge stations (i.e., Danang and Tramy). Other stations including Ainghia, Camle, Gioathuy, Cau Lau, Hien, Hiepduc, Hoian, Khamduc, Nongson, Queson, Thanhmy and Tienphuoc are popular rain gauge stations which operate manually on the base of volunteers. The location of these stations is displayed on Figure 1. The data is available from 1986–2015.

### 2.2.2. Gridded Data

The precipitation products are from different assemblies of regional models: (1) The Regional Climate Model version 4 (RegCM4), developed by the International Centre for Theoretical Physics (ICTP). The dynamical structure of RegCM4 firstly developed at the National Center of Atmosphere Research (NCAR) and Penn State University (PSU) for a hydrostatic version of the Meso-scale Model (MM5). A detailed description of RegCM4 can be found in Giorgi et al. [31]. The model output of HadGEM2-AO produced by the National Institute of Meteorological Research (NIMR)/Korea Meteorological Administration (KMA) are used as an initial and boundary conditions, referred to REG/HadGEM. Details of HadGEM2-AO are given by Collins et al. [32]; (2) The model of SNU-MM5 (Seoul National University Meso-scale Model version 5) [33] is based on a hydrostatic version of the Meso-scale Model and the community land model version 3 (CLM3). The future climatic projections are produced with the HadGEM2-AO, referred to SNU/HadGEM; (3) A regional spectral model, which is also known as Regional Model Program (RMP) of the Global/Regional Integrated Model System (GRIMs) [34] is used in this study. The dynamic frame of RMP is rooted in the National Center for Environmental Prediction (NCEP) RSM. More detailed information about the GRIMs-RMP is provided by Hong et al. [34]. This model is driven by the HadGEM2-AO, referred to RSM/HadGEM; (4) The RegCM4 is forced by the model of Max Planck Institute for Meteorology Earth System Model MR (MPI-ESM-MR), which has an ocean horizontal resolution of  $0.4^\circ \times 0.4^\circ$  and atmosphere horizontal resolution of  $1.9^\circ \times 1.9^\circ$ . It is written under a short symbol of REG/MPI; (5) The RegCM4 is forced by

the model of Institut Pierre Simon Laplace CM5A-LR (IPSL-CM5A-LR), which is the low-resolution version of the IPSL-CM5A Earth system model. It has a horizontal resolution of  $1.875^\circ \times 3.75^\circ$  with 39 vertical level for the atmosphere and about  $2^\circ$  (with a meridional increased resolution of  $0.5^\circ$  near the equator) and with 31 vertical levels for the ocean. In this study, it implies to REG/IPSL; (6) The RegCM4 is forced by the model of Irish Centre for High-End Computing European community Earth-System (ICHEC-EC-EARTH), which is a new Earth system model on the basic of the operational seasonal forecast system of the European Centre for Medium-Range Weather Forecasts (ECMWF). This case is written with a short symbol of the REG/ICHEC. More importantly, all simulations and projections of climatic are run under two IPCC RCP4.5/8.5 scenarios. The RCP4.5 is a stabilization scenario where total radiative forcing is stabilized before 2100 by employment of a range of technologies and strategies for reducing greenhouse gas emissions. Meanwhile, the RCP8.5 is characterized by increasing greenhouse gas emissions over time representative for scenarios in the literature leading to high greenhouse gas concentration. Table 1 lists the name of the models and the number of runs of historical control and RCPs as well as the considered periods. A total of 18 climatic simulations and projections are considered in this study as shown in Table 1.

**Table 1.** Climate models and number of runs.

	Historical (1986–2005)	RCP4.5 (2021–2050)	RCP8.5 (2021–2050)	Spatial Resolution	Temporal Resolution
RegCM4 forced by MPI-ESM-MR (REG/MPI)	1	1	1	20 km	Monthly
RegCM4 forced by IPSL-CM5A-LR (REG /IPSL)	1	1	1	20 km	Monthly
RegCM4 forced by ICHEC-EC-EARTH (REG/ICHEC)	1	1	1	20 km	Monthly
RegCM4 forced by HadGEM2-AO (REG/HadGEM)	1	1	1	20 km	Monthly
SNU-MM5 forced by HadGEM2-AO (SNU/HadGEM)	1	1	1	20 km	Monthly
RSM forced by HadGEM2-AO (RSM/HadGEM)	1	1	1	20 km	Monthly

### 2.3. Methods

#### 2.3.1. Delta Change Factor

The raw climate simulations, especially for precipitation time series, are highly biased as mentioned in many studies [6,35,36]. Thus, an additional post-processing step (e.g., bias correction of climatic variables) is a standard procedure for related climate change studies. In this study, the delta change method is adopted due to its simple and common use as described in Olsso et al. [37], Lenderink et al. [38], Teutschbein and Seibert [36] and Maraun [35]. This approach does not adjust the output of climate models, but uses observations and the change signal of regional climate models forced by global climate models to generate future data. Also, this approach is to avoid considerable variability in the day-to-day change signals and changes in extremes are linearly scaled with changes in the mean. The core of this method is that the historical observations are transformed into future projections using

monthly average correction factors that derived from the regional climate models forced by global climate model outputs for the baseline and future climate. It is expressed by the equation:

$$P_{OBS,f} = \frac{\overline{P_{GCM,f}}}{\overline{P_{GCM,b}}} \cdot P_{OBS,b} \quad (1)$$

where  $\overline{P_{GCM,f}}$  is the monthly precipitation from the future climate.  $\overline{P_{GCM,b}}$  is the monthly precipitation from the baseline climate.  $P_{OBS,f}$  is future projections and  $P_{OBS,b}$  is historical observations.

With this approach, the correlation structure of downscaled future data in spatio-temporal terms are physically reasonable because it reflects observed conditions. The drawback of this approach, however, is that the future and baseline scenarios just differ in terms of their means and intensity, but other statistics of the data (e.g., skewness or structure of dry and wet days) are mostly unchanged. Also, the sample is limited to the length of the observed record. It should be noted that for a near-term future (2021–2050), the changes in the dry/wet days are probably trivial. Sun et al. [39] used the lag 1 autocorrelation to investigate the stationary land-based gridded annual precipitation (1940–2009). The results showed a stationary annual precipitation over an area of about 80% of the global land surface. Wilks and Wilby [40] show that calculating the autocorrelation of non-zero precipitation amounts is essential at time step of hourly (or sub-hourly) rather than a daily time step. Meanwhile, the autocorrelation between successive nonzero precipitation amounts is usually of little practical importance and quite small. At a time step of monthly precipitation, thus, a stationary assumption in the temporal correlation is made in this study. In other words, rescaling the precipitation time series observed during the baseline could lead to not realistic results when future scenarios that preserve the observed autocorrelation in time are not considered.

### 2.3.2. Unequal Weights

In this study, a method is suggested to estimate the unequal weights based on the rank sum from each climate simulation run for the analytical hierarchy process. It is called unequal weights. The rank sum is calculated using the statistical indices. The statistical indices are Nash–Sutcliffe efficiency with logarithmic value ( $\ln(\text{Nash})$ ), root-mean-square error (RMSE) and Nash–Sutcliffe efficiency (Nash) for the studied domain. They are basically quantified by measuring the difference between the observed data and the outputs of regional climate models forced by lateral and surface boundary conditions from the European Centre for Medium-Range Weather Forecasts at the monthly scale. The Nash–Sutcliffe efficiency with logarithmic values  $\ln(\text{Nash})$  is selected because it can be added to expect a better quantification of the performance in different conditions (maximum and minimum values) [41]. The other remaining value is widely applied in hydrometeorological fields. The formulations used to compute the goodness-of-fit statistical indicators for each climate simulation run are presented as follows:

$$\text{RMSE} = \sqrt{\frac{1}{n} \sum_{i=1}^n (F_i - O_i)^2} \quad (2)$$

$$\ln(\text{Nash}) = 1 - \frac{\sum_1^n (\ln O_i - \ln F_i)^2}{\sum_1^n (\ln O_i - \ln \bar{O})^2} \quad (3)$$

$$\text{Nash} = 1 - \frac{\sum_1^n (O_i - F_i)^2}{\sum_1^n (O_i - \bar{O})^2} \quad (4)$$

where  $n$  denotes number of months,  $F_i$  and  $O_i$  represent simulated and observed monthly data, respectively. The method of unequal weights is briefly expressed with the following steps with an assumption of  $N$  climate simulations:

- (1) Calculation of the statistical indices on the basic of the historical observations and climate simulations from regional climate models forced by the reanalysis data of the European Centre

for Medium-Range Weather Forecasts during 1989–2008. Each climate simulation receives a rank from 1 to  $N$  depending on the levels of perfect score for each statistical index, starting with the best as 1 and the worst is  $N$ . As an example, if the RMSE index of the  $i$ th climate model has the best score (the perfect score of RMSE is zero), the received rank is 1. Then, an ensemble rank order ( $r$ ) as an integer number is calculated from the average of the ranks they span for each climate simulation.

- (2) Calculation of rank sum for each climate simulation by  $N-r + 1$  with  $N$  is the number of climate simulations.
- (3) Establishing a reciprocal matrix between sets of models  $a_{ij} = 1/a_{ji}$  with  $i, j$  ranging from 1 corresponding to the best climate simulation which has the largest rank sum to  $N$  and  $a_{ij} = 1$  as  $i = j$ .  $a_{ij}$  is determined by the difference of rank sum between sets of models plus 1.
- (4) Estimation of weights matrix  $w_{ij} = a_{ij} / \sum_{j=1}^N a_{ij}$  ( $i, j = 1, N$ )
- (5) Estimation of each weight for each climate simulation  $w_i = \sum_{j=1}^N w_{ji}$  ( $i = 1, N$ ) with  $\sum_{i=1}^N w_i = 1$ .

### 2.3.3. Standardized Precipitation Index (SPI)

In this study, the SPI is constructed for multiple timescales ranging from 1 month to 24 months. The calculation of the SPI is separately applied for each month on the basis of the Gamma distribution. The reason for this is that the Gamma distribution is the most frequently used and fits well with daily precipitation in different studies across Vietnam [42]. The alpha and beta parameters of the Gamma probability density function are estimated for each station and for the required multiple timescales. They are used to calculate the cumulative probability distribution of accumulated precipitation. The maximum likelihood solutions [43] and Thom's study [44] are applied to optimally estimate alpha ( $\alpha$ ) and beta ( $\beta$ ). It is especially noteworthy that the reference period adopted to compute the best-fit parameters for the gamma distribution spans 30 years (1986–2015).

A probability transformation is then applied to transform monthly precipitation to a standard normal distribution with a zero mean and standard deviation of one to yield SPI values by preserving probabilities [45]. Figure 2 shows the fitness of the SPI data [46].

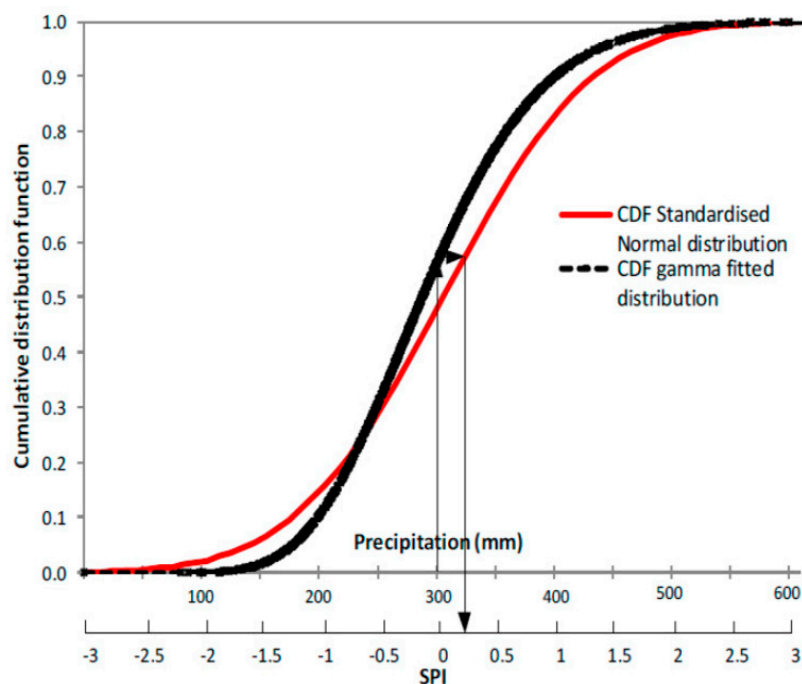


**Figure 2.** The probability transformation from fitted gamma distribution to the standard normal distribution.

### 2.3.4. Non-Parametric Mann–Kendall Test

The non-parametric Mann–Kendall (MK) test [25,26] is widely applied to detect the possible trends in many countries such as in China [47], in Serbia [48] in Brazil [49], in Canada [50]. In this study, the MK test statistic,  $S$ , is applied and briefly represented by:

$$S = \sum_k^{n-1} \sum_{j=k+1}^n \text{sign}(x_j - x_k) \tag{5}$$

where  $n$  is the number of data points;  $x_j$  and  $x_k$  are the data values in time series  $j$  and  $k$  respectively, and

$$\text{sign}(x_j - x_k) = \begin{cases} +1 & \text{if } x_j - x_k > 0 \\ 0 & \text{if } x_j - x_k = 0 \\ -1 & \text{if } x_j - x_k < 0 \end{cases} \tag{6}$$

In this test, the null hypothesis ( $H_0$ ) assumes that there is no trend in meteorological droughts over time; the alternative hypothesis ( $H_1$ ) assumes that there is an upward or downward trend over time. The mathematical equations for calculating  $\text{Var}(S)$  and standardized test statistics  $Z$  are presented in previous studies [25,26,47,51,52]. An upward, downward, or no trend will be assessed at  $\alpha$  significance level of 0.05. The computed probability is greater than the specific significance level  $\alpha$  ( $H_0$  is rejected); the increasing trend responds to a positive value of  $Z$  and a negative value of  $Z$  indicates a decreasing trend. There is no trend if the computed probability is less than the level of significance ( $H_0$  is accepted). At the  $\alpha$  significance level of 0.05, the null hypothesis of no trend is rejected if  $|Z_{MK}| > 1.96$ .

### 2.3.5. The Sen’s Slope Estimator

In order to get the magnitude of a consistent trend ( $Q$ ), the Sen’s non-parametric method [19] is used. It is estimated by the slope of all data pairs ( $N = n(n - 1)/2$ ) as the following formula:

$$Q_i = \frac{x_j - x_k}{j - k} \text{ for } i = 1, N \tag{7}$$

where  $Q$  is slope between data points  $x_j$  and  $x_k$ ,  $x_j$  and  $x_k$  are the data values at time  $j$  and  $k$  ( $j > k$ ) respectively,  $j$  is time after time  $k$ . The Sen’s is computed by the median slope as:

$$Q_{\text{med}} = \begin{cases} Q_{[\frac{N+1}{2}]} & \text{if } N \text{ is odd} \\ \frac{Q_{[\frac{N}{2}]} + Q_{[\frac{N+2}{2}]}}{2} & \text{if } N \text{ is even} \end{cases} \tag{8}$$

where  $N$  is the number of calculated slopes.

The confidence limits for the nonparameter slope estimator are estimated by the well-known studies [27,29,53,54].

## 3. Results and Discussions

### 3.1. Calculation of Weights for Each Climate Model

As the first step, the delta change factor is applied in this study. Then, the unequal weights are added to define weights for each climate simulations as mentioned in Table 1 over the whole VG-TB. Table 2 shows the statistical indices for these climate simulations. For RMSE index, the perfect score is zero with a wide range ( $0 \leq \text{RMSE} < \infty$ ). While the perfect score of Nash and  $\ln(\text{Nash})$  indices is 1 with a wide span ( $-\infty \leq \text{Nash} < 1$ ;  $-\infty \leq \ln(\text{Nash}) < 1$ ). Based on these score, ranks (i.e., ensemble rank, rank sum) are calculated and presented in Table 3. It is observed that REG/IPSL gives the best score of  $\ln(\text{Nash})$ , RMSE and Nash. This means that REG/IPSL simulation is well matched to observations.

As opposed to this, RSM/HadGEM gives the worst score of In(Nash), RMSE and Nash. Although REG/IPSL is the best, a multiple climate model is always highlighted in the climate simulations and projections due to reducing uncertainty [7]. The reason for this is that the uncertainty comes from lots of factors such as convective cloud parameterization, greenhouse gases scenarios or land surface parameterization. The best rank sum belongs to the model REG/IPSL, followed by REG/ICHEC. In contrary to this, the worst rank sum belongs to the model RSM/HadGEM as shown in Table 3.

**Table 2.** Statistical indices for multiple climate models.

	In(Nash)	RMSE	Nash
REG/ICHEC	0.935	170.67	0.523
REG/IPSL	0.941	157.44	0.594
REG/MPI	0.937	171.90	0.516
REG/HadGEM	0.891	256.72	−0.079
SNU/HadGEM	0.913	252.75	−0.046
RSM/HadGEM	0.880	278.93	−0.274

**Table 3.** Ranks of climate models.

	In(Nash)	RMSE	Nash	Average	Ensemble Rank	Rank Sum
REG/ICHEC	3	2	2	2.3	2	5
REG/IPSL	1	1	1	1.0	1	6
REG/MPI	2	3	3	2.7	3	4
REG/HadGEM	5	5	4	4.7	5	2
SNU/HadGEM	4	4	5	4.3	4	3
RSM/HadGEM	6	6	6	6.0	6	1

A reciprocal matrix between sets of models is created based on the rank sum of climate models. As shown in Table 4, it is illustrated that REG/IPSL is more important than REG/ICHEC and much more important than REG/MPI. Meanwhile, REG/ICHEC is more important than REG/MPI and much important than SNU/HadGEM. The least importance within all considered climate simulations is RSM/HadGEM, followed by REG/HadGEM.

**Table 4.** A reciprocal matrix between sets of models.

	REG/IPSL	REG/ICHEC	REG/MPI	SNU/HadGEM	REG/HadGEM	RSM/HadGEM	Total
REG/IPSL	1	2	3	4	5	6	21
REG/ICHEC	1/2	1	2	3	4	5	15.5
REG/MPI	1/3	1/2	1	2	3	4	10.83
SNU/HadGEM	1/4	1/3	1/2	1	2	3	7.08
REG/HadGEM	1/5	1/4	1/3	1/2	1	2	4.28
RSM/HadGEM	1/6	1/5	1/4	1/3	1/2	1	2.45
<b>Total</b>							<b>61.15</b>

After establishing a weights matrix, weights are estimated for each climate model based on the 4th and 5th steps in Section 2.3.2. Weights are 0.344 (REG/IPSL), 0.254 (REG/ICHEC), 0.177 (REG/MPI), 0.116 (SNU/HadGEM), 0.07 (REG/HadGEM) and 0.038 (RSM/HadGEM). The results from this method are against the results from the method of equal weights. Both of them are compared with observations using the statistical indices of mean absolute error (MAE) and RMSE. The pair of equal weights and observations gives results of 99.3 for MAE and 164 for RMSE, meanwhile a pair of unequal weights and observations gives results of 95.4 and 155 for MAE and RMSE, respectively.

The perfect score of MAE and RMSE is zero. In other words, the minimum of the RMSE and MAE is obtained when simulated time series perfectly matches observed time series. As mentioned in the delta change factor approach, an assumption of the delta factor is equal to one (i.e., there is no variation) for each climate runs, and the condition of minimum of the RMSE and MAE is obtained.

Climate models with convective precipitation schemes, however, often tend to produce higher precipitation [6,55] compared with the observed data. Moreover, incomplete understanding of natural and its representation is presented within the climate models. Thus, the delta factor assumed by one is unreal, especially in Vietnam where the rain regime is strongly dominated by convective processes. The calculated statistics of MAE and RMSE indicate a better implementation of unequal weights. Climate simulations are closely fit to observations with the unequal weights method as presented in Figure 3.

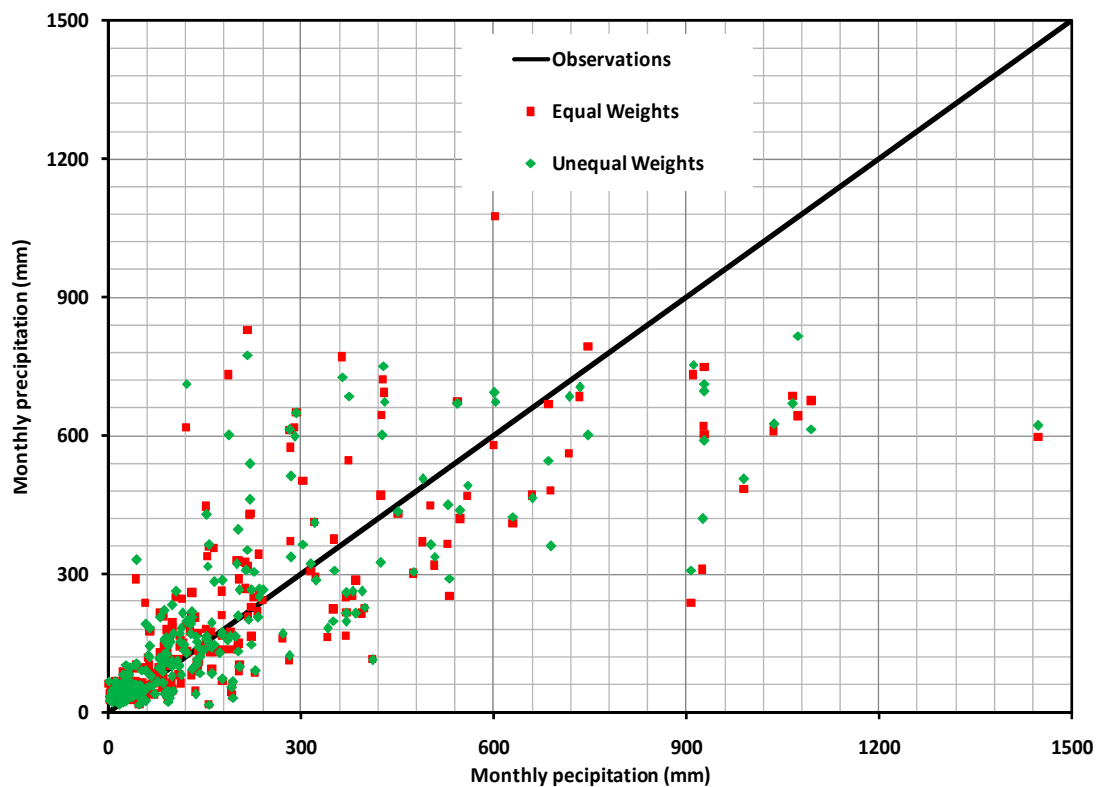


**Figure 3.** Scatter plot of the precipitation simulations with equal and unequal weights minus observations over the whole VG-TB during 1989–2008 (mm/month).

### 3.2. Calculation of SPI

The weights estimated from Section 3.1 are used to calculate the SPI for 14 stations over the whole VG-TB. It is noted that the weights are applied for both scenarios of RCP4.5 and RCP8.5 during 2021–2050 with an assumption of no change in future. The SPI is designed to project the precipitation deficit for multiple timescales with a weighted ensemble of multiple climate models in future. SPI values are computed for the timescales of 1- (SPI-1), 3- (SPI-3), 6- (SPI-6), 9- (SPI-9), 12- (SPI-12) and 24- (SPI-24) month for 14 stations. For instance, the temporal variation of drought for the timescales of 1 to 24 months under RCP4.5 (Figure 4) and RCP8.5 (Figure 5) at Danang station from 2021 to 2050 is displayed.

According to the classification of SPI values [56], generally, there are no events classified as “extremely wet” and “extremely dry” for the Danang station under both scenarios of RCP4.5 and RCP8.5 during 2021–2050 for considered multiple timescales. Under these scenarios, events classified as “near normal” hold more than 90% out of considered months for all timescales of 14 stations. In particular, events classified as “extremely wet” and “extremely dry” are not found out for the all stations under both scenarios of RCP4.5 and RCP8.5 during 2021–2050 for SPI-1, SPI-3, SPI-6, SPI-9, SPI-12 and SPI-24 indices. More importantly, under RCP4.5 scenario, events classified as “very wet” and “severely dry” are lower than 0.6% (mainly in stations located in the east of basin

as Caulau) (see Supplementary Material). Meanwhile there is a little change (less than 2.8%) in events classified as “very wet”, “moderately wet”, “moderately dry” and “severely dry” for SPI-1 for Ainghia, Camle, Giaothuy, Danang and Hien stations under the RCP8.5 scenario. Under this scenario, the remaining stations have no change in drought and wet events for all considered multiple time scales (see Supplementary Material). This indicates only little changes in drought and wet events in the eastern domain of basin under RCP8.5 for considered time scales. “Moderately wet” events for the SPI-1 range from 1.4% (Hien, Hoian and Khamduc stations) to 2.8% (Danang station) under the RCP4.5 scenario. Hence, an emphasis of events classified as “moderately wet” and “moderately dry” for multiple timescales over the whole basin under the RCP4.5 scenario during 2021–2050 is documented in Table 5.

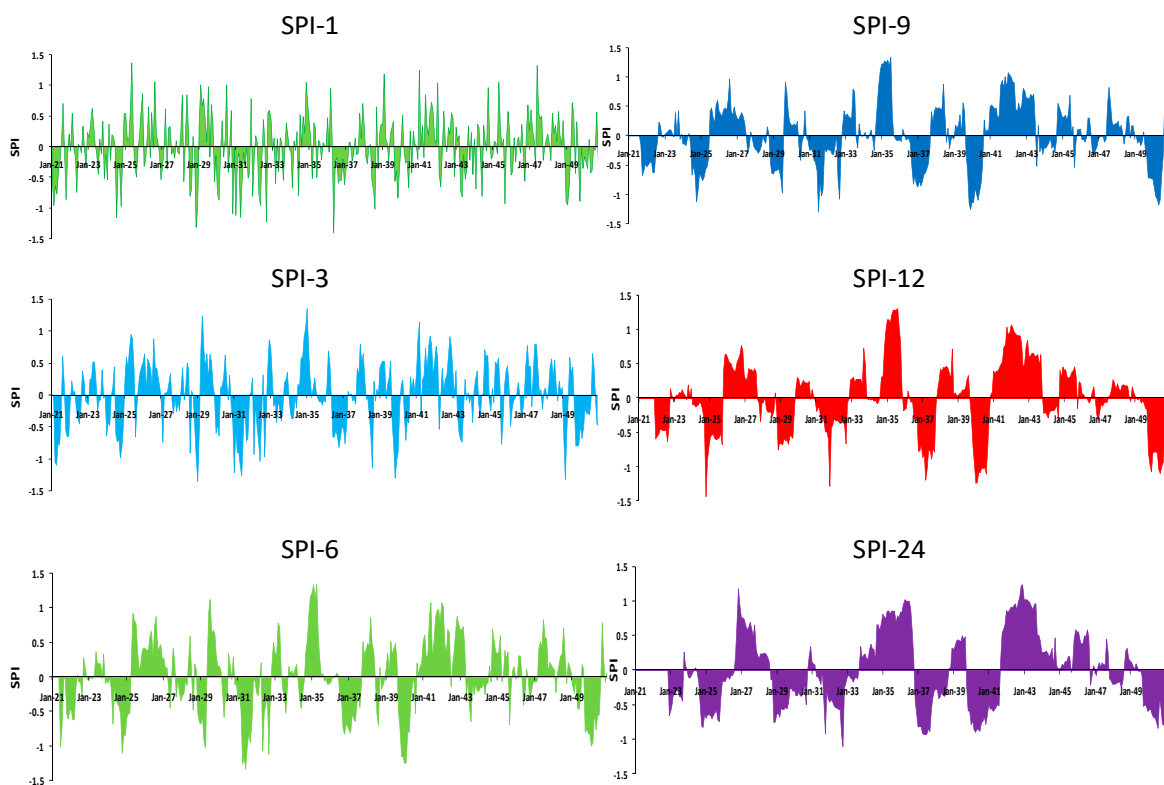


**Figure 4.** Standardized precipitation index (SPI) for multiple timescales under RCP4.5 scenario (2021–2050) for Danang station.

As shown in Table 5, the maximum of moderately dry event is 6.5% for SPI-24, followed by 6.3% and 6.0% for SPI-12 and SPI-9, respectively. The median of moderately dry is projected to get the maximum value of 4.2% for SPI-24, followed by 4.0% and 3.7% for SPI-9 and SPI-12, respectively. Importantly, the maximum of moderately wet event is 5.9% for SPI-24, followed by 3.7% and 3.4% for SPI-12 and SPI-9, respectively. It is noteworthy that the values reported from Table 5 and Tables S1–S6 are assigned by the percentages of drought and wet events under considered multiple timescales. In other words, these values are defined as the percentage of number of months suffering wet and drought events among all months during a 30-year period under considered scenarios. Under the RCP4.5 scenario, in general, timescales are longer, intensity of moderately dry is stronger. In the same timescale, occurrence of moderately wet events is smaller than that of moderately dry under RCP4.5 scenario during 2021–2050.

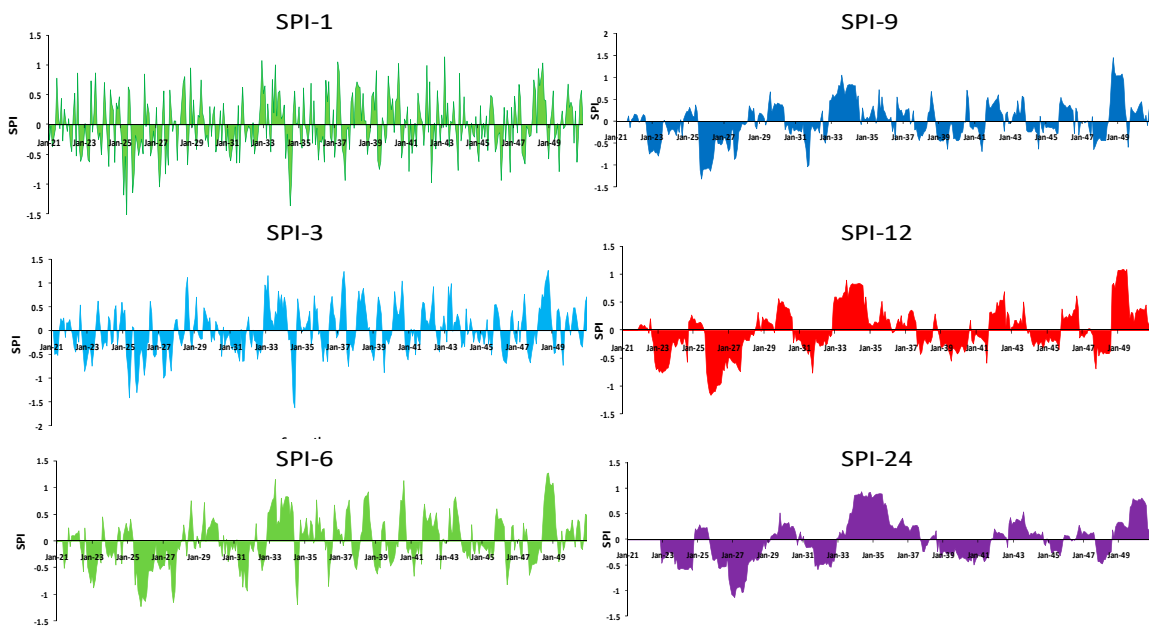


Figure 5. SPI for multiple timescales under RCP8.5 scenario (2021–2050) for Danang station.

Table 5. Percentages of drought and wet events under considered multiple timescales under RCP4.5 scenario over basin during 2021–2050 (%).

	Classification	Min	25%	Median	75%	Max
SPI-1	Moderately wet	1.4	1.5	2.1	2.2	2.8
	Moderately dry	1.4	1.7	2.1	2.2	3.1
SPI-3	Moderately wet	0.8	1.2	1.4	1.9	2.2
	Moderately dry	1.1	2.6	3.1	3.4	3.9
SPI-6	Moderately wet	0.6	1.1	1.3	1.9	2.5
	Moderately dry	1.4	3.7	3.8	4.2	5.1
SPI-9	Moderately wet	0.3	0.3	1.3	2.4	3.4
	Moderately dry	1.7	3.3	4.0	4.5	6.0
SPI-12	Moderately wet	0.0	0.3	0.7	1.8	3.7
	Moderately dry	0.9	3.2	3.7	4.4	6.3
SPI-24	Moderately wet	0.3	1.8	2.4	3.5	5.9
	Moderately dry	0.0	0.4	4.2	5.5	6.5

### 3.3. Projection Trends in SPI

Projection trends in SPI for multiple timescales are considered with an emphasis of drought events under the RCP4.5 scenario. The purpose of this is to detect any trends or changes in drought events. In addition, as clarified in the previous section, just little, even no wet and drought events of extremely wet, extremely dry, very wet and severely dry are found out under the RCP8.5 scenarios. During 2021–2050, out of 14 stations, only five show significant upward trends in November for the SPI-1 index as presented in Figure 6b. There is a similar of upward trends for SPI-3 and SPI-6 in November. Importantly, no trends are detected in November for SPI-9, SPI-12 and SPI-24. Besides that, it is noteworthy that a poor signal of upward trends in SPI-9, SPI-12 and SPI-24 indices is illustrated for months in a year. It indicates an importance of short-term, plans more than long-term plans in related aspects such as water resources planning.

In February, insignificant downward trends are mostly observed over the whole basin (Figure 6a). In the months of March, May, July, October and December, more than half of total considered stations are defined with no trends in SPI-1 index. No trends in SPI-3 index are calculated for almost all the

months in a year, except for January, April and November. Downward trends in SPI-1 (in the months of February, April and June), SPI-3 (in April) and SPI-6 (in the months of July and August) indices are clearly observed. More importantly, the intensity of drought events in the north and east of the basin is generally stronger than that in other areas.

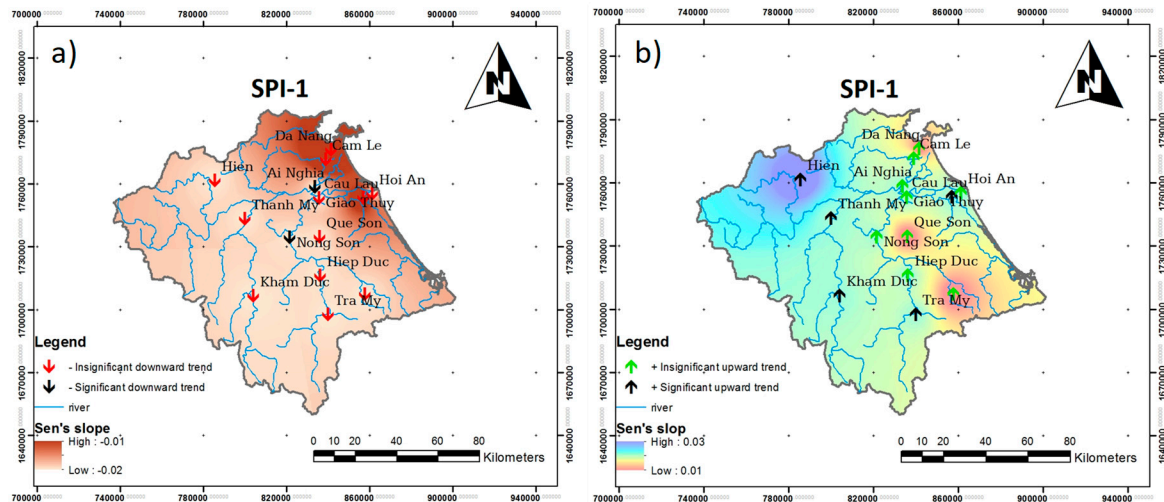


Figure 6. Spatial distribution of Sen's slope in February (a) and in November (b) for SPI-1 index.

#### 4. Conclusions

This study presents a proposed approach to evaluate drought characteristics using multiple climate models for multiple timescales under a context of global warming. The method of unequal weights is proposed to reduce uncertainty of climate projections. The Mann–Kendall and Sen's slope methods are then applied to find the trends in drought characteristics for multiple timescales of 1, 3, 6, 9, 12, and 24 months with six climate projections. The unequal weights are proposed on the basis of rank sum of each climate model. Vu Gia–Thu Bon basin located in central Vietnam is selected to implement this study as a pilot basin. The major findings of the present study can be exposed as an impulse of the precipitation simulations using unequal weights for multiple climate models. Under the scenarios of RCP4.5 and RCP8.5, there are no events classified as “extremely wet” and “extremely dry” for the all stations during 2021–2050 for SPI-1, SPI-3, SPI-6, SPI-9, SPI-12 and SPI-24 indices. A higher magnitude of the drought conditions in the north and east of the basin compared to other areas is found out. Under the RCP4.5 scenario, more importantly, timescales are longer, and the intensity of moderately dry is stronger. Moreover, the occurrence of moderately wet events is smaller than that of moderately dry under the RCP4.5 scenario during 2021–2050 in the same timescales. Under the RCP8.5 scenario, events classified as “extremely wet”, “extremely dry”, “very wet” and “severely dry” are expected to rarely occur.

**Supplementary Materials:** The following are available online at <http://www.mdpi.com/2225-1154/6/4/79/s1>.

**Funding:** This research received no external funding.

**Conflicts of Interest:** The author declares no conflicts of interest.

#### References

1. Weigel, A.P.; Knutti, R.; Liniger, M.A.; Appenzeller, C. Risks of model weighting in multimodel climate projections. *J. Clim.* **2010**, *23*, 4175–4191. [[CrossRef](#)]
2. Moreland, J. *Drought: Us Geological Survey Water Fact Sheet*; Open-File Report; U.S. Geological Survey: Reston, VA, USA, 1993; pp. 93–642.

3. Dracup, J.A.; Lee, K.S.; Paulson, E.G., Jr. On the definition of droughts. *Water Resour. Res.* **1980**, *16*, 297–302. [[CrossRef](#)]
4. Wilhite, D.A.; Glantz, M.H. Understanding: The drought phenomenon: The role of definitions. *Water Int.* **1985**, *10*, 111–120. [[CrossRef](#)]
5. WMO. *Standardized Precipitation Index—User Guide*; WMO-No. 1090; WMO: Geneva, Switzerland, 2012.
6. IPCC. *Climate Change 2007—The Physical Science Basis: Working Group I Contribution to the Fourth Assessment Report of the IPCC*; Cambridge University Press: Cambridge, UK, 2007; Volume 4.
7. IPCC. *Climate Change 2013: The Physical Science Basis: Working Group I Contribution to the Fifth Assessment Report of the Intergovernmental Panel on Climate Change*; Cambridge University Press: Cambridge, UK, 2014.
8. Svoboda, M.; Fuchs, B. *Handbook of Drought Indicators and Indices*; WMO-No. 1173; WMO: Geneva, Switzerland, 2016.
9. Svoboda, M.; LeComte, D.; Hayes, M.; Heim, R.; Gleason, K.; Angel, J.; Rippey, B.; Tinker, R.; Palecki, M.; Stooksbury, D. The drought monitor. *Bull. Am. Meteorol. Soc.* **2002**, *83*, 1181–1190. [[CrossRef](#)]
10. Vogt, J.; Barbosa, P.; Hofer, B.; Magni, D.; Jager, A.; Singleton, A.; Horion, S.; Sepulcre, G.; Micale, F.; Sokolova, E. *Developing a European Drought Observatory for Monitoring, Assessing and Forecasting Droughts across the European Continent*; AGU Fall Meeting Abstracts; Copernicus Publications: Göttingen, Germany, 2011.
11. Anctil, F.; Larouche, W.; Viau, A.; Parent, L.-E. Exploration of the standardized precipitation index with regional analysis. *Can. J. Soil Sci.* **2002**, *82*, 115–125. [[CrossRef](#)]
12. Salehnia, N.; Alizadeh, A.; Sanaeinejad, H.; Bannayan, M.; Zarrin, A.; Hoogenboom, G. Estimation of meteorological drought indices based on agmerra precipitation data and station-observed precipitation data. *J. Arid Land* **2017**, *9*, 797–809. [[CrossRef](#)]
13. Ntale, H.K.; Gan, T.Y. Drought indices and their application to East Africa. *Int. J. Climatol.* **2003**, *23*, 1335–1357. [[CrossRef](#)]
14. Vicente-Serrano, S.M.; Beguería, S.; López-Moreno, J.I. A multiscalar drought index sensitive to global warming: The standardized precipitation evapotranspiration index. *J. Clim.* **2010**, *23*, 1696–1718. [[CrossRef](#)]
15. Palmer, W.C. *Meteorological Drought*; Research Paper No. 45; US Department of Commerce Weather Bureau: Washington, DC, USA, 1965; p. 59.
16. Wells, N.; Goddard, S.; Hayes, M.J. A self-calibrating palmer drought severity index. *J. Clim.* **2004**, *17*, 2335–2351. [[CrossRef](#)]
17. Tsakiris, G.; Pangalou, D.; Vangelis, H. Regional drought assessment based on the reconnaissance drought index (rdi). *Water Resour. Manag.* **2007**, *21*, 821–833. [[CrossRef](#)]
18. Spinoni, J.; Naumann, G.; Carrao, H.; Barbosa, P.; Vogt, J. World drought frequency, duration, and severity for 1951–2010. *Int. J. Climatol.* **2014**, *34*, 2792–2804. [[CrossRef](#)]
19. Weisheimer, A.; Doblas-Reyes, F.; Palmer, T.; Alessandri, A.; Arribas, A.; Déqué, M.; Keenlyside, N.; MacVean, M.; Navarra, A.; Rogel, P. Ensembles: A new multi-model ensemble for seasonal-to-annual predictions—Skill and progress beyond demeter in forecasting tropical pacific ssts. *Geophys. Res. Lett.* **2009**, *36*. [[CrossRef](#)]
20. DelSole, T.; Yang, X.; Tippett, M.K. Is unequal weighting significantly better than equal weighting for multi-model forecasting? *Q. J. R. Meteorol. Soc.* **2013**, *139*, 176–183. [[CrossRef](#)]
21. Sanderson, B.M.; Wehner, M.; Knutti, R. Skill and independence weighting for multi-model assessments. *Geosci. Model Dev.* **2017**. [[CrossRef](#)]
22. Knutti, R.; Abramowitz, G.; Collins, M.; Eyring, V.; Gleckler, P.J.; Hewitson, B.; Mearns, L.O. Good Practice Guidance Paper on Assessing and Combining Multi Model Climate Projections. In Proceedings of the IPCC Expert Meeting on Assessing and Combining Multi Model Climate Projections, Boulder, CO, USA, 28–27 January 2010; p. 1.
23. Krishnamurti, T.N.; Kishtawal, C.; Zhang, Z.; LaRow, T.; Bachiochi, D.; Williford, E.; Gadgil, S.; Surendran, S. Multimodel ensemble forecasts for weather and seasonal climate. *J. Clim.* **2000**, *13*, 4196–4216. [[CrossRef](#)]
24. Taylor, K.E.; Stouffer, R.J.; Meehl, G.A. An overview of cmip5 and the experiment design. *Bull. Am. Meteorol. Soc.* **2012**, *93*, 485–498. [[CrossRef](#)]
25. Kendall, M.G. *Rank Correlation Methods*; Hafner Publishing Co.: Oxford, UK, 1955.
26. Mann, H.B. Nonparametric tests against trend. *Econ. J. Econ. Soc.* **1945**, 245–259. [[CrossRef](#)]
27. Sen, P.K. Estimates of the regression coefficient based on kendall’s tau. *J. Am. Stat. Assoc.* **1968**, *63*, 1379–1389. [[CrossRef](#)]

28. Douglas, E.; Vogel, R.; Kroll, C. Trends in floods and low flows in the united states: Impact of spatial correlation. *J. Hydrol.* **2000**, *240*, 90–105. [[CrossRef](#)]
29. Helsel, D.R.; Hirsch, R.M. *Statistical Methods in Water Resources*; Elsevier: New York, NY, USA, 1992; Volume 49.
30. Hirsch, R.M.; Slack, J.R.; Smith, R.A. Techniques of trend analysis for monthly water quality data. *Water Resour. Res.* **1982**, *18*, 107–121. [[CrossRef](#)]
31. Giorgi, F.; Coppola, E.; Solmon, F.; Mariotti, L.; Sylla, M.; Bi, X.; Elguindi, N.; Diro, G.; Nair, V.; Giuliani, G. Regcm4: Model description and preliminary tests over multiple cordex domains. *Clim. Res.* **2012**, *52*, 7–29. [[CrossRef](#)]
32. Collins, W.; Bellouin, N.; Doutriaux-Boucher, M.; Gedney, N.; Halloran, P.; Hinton, T.; Hughes, J.; Jones, C.; Joshi, M.; Liddicoat, S. Development and evaluation of an earth-system model—Hadgem2. *Geosci. Model Dev.* **2011**, *4*, 1051–1075. [[CrossRef](#)]
33. Lee, D.-K.; Cha, D.-H.; Kang, H.-S. Regional climate simulation of the 1998 summer flood over East Asia. *J. Meteorol. Soc. Jpn. Ser. II* **2004**, *82*, 1735–1753. [[CrossRef](#)]
34. Hong, S.-Y.; Park, H.; Cheong, H.-B.; Kim, J.-E.E.; Koo, M.-S.; Jang, J.; Ham, S.; Hwang, S.-O.; Park, B.-K.; Chang, E.-C. The global/regional integrated model system (grims). *Asia-Pac. J. Atmos. Sci.* **2013**, *49*, 219–243. [[CrossRef](#)]
35. Maraun, D. Bias correcting climate change simulations—A critical review. *Curr. Clim. Chang. Rep.* **2016**, *2*, 211–220. [[CrossRef](#)]
36. Teutschbein, C.; Seibert, J. Is bias correction of regional climate model (rcm) simulations possible for non-stationary conditions? *Hydrol. Earth Syst. Sci.* **2013**, *17*, 5061–5077. [[CrossRef](#)]
37. Olsson, J.; Berggren, K.; Olofsson, M.; Viklander, M. Applying climate model precipitation scenarios for urban hydrological assessment: A case study in Kalmar City, Sweden. *Atmos. Res.* **2009**, *92*, 364–375. [[CrossRef](#)]
38. Lenderink, G.; Buishand, A.; Deursen, W.V. Estimates of future discharges of the river rhine using two scenario methodologies: Direct versus delta approach. *Hydrol. Earth Syst. Sci.* **2007**, *11*, 1145–1159. [[CrossRef](#)]
39. Sun, F.; Roderick, M.L.; Farquhar, G.D. Rainfall statistics, stationarity, and climate change. *Proc. Natl. Acad. Sci. USA* **2018**, *115*, 2305–2310. [[CrossRef](#)] [[PubMed](#)]
40. Wilks, D.S.; Wilby, R.L. The weather generation game: A review of stochastic weather models. *Prog. Phys. Geogr.* **1999**, *23*, 329–357. [[CrossRef](#)]
41. Krause, P.; Boyle, D.; Båse, F. Comparison of different efficiency criteria for hydrological model assessment. *Adv. Geosci.* **2005**, *5*, 89–97. [[CrossRef](#)]
42. Nguyen, T.T.; Remo, L.D.A. Projected changes of precipitation idf curves for short duration under climate change in central Vietnam. *Hydrology* **2018**, *5*, 33.
43. Choi, S.C.; Wette, R. Maximum likelihood estimation of the parameters of the gamma distribution and their bias. *Technometrics* **1969**, *11*, 683–690. [[CrossRef](#)]
44. Thom, H.C. A note on the gamma distribution. *Mon. Weather Rev.* **1958**, *86*, 117–122. [[CrossRef](#)]
45. Edwards, D.C. *Characteristics of 20th Century Drought in the United States at Multiple Time Scales*; Air Force Inst of Tech: Wright-Patterson AFB, OH, USA, 1997.
46. Azam, M.; Maeng, S.; Kim, H.; Lee, S.; Lee, J. Spatial and temporal trend analysis of precipitation and drought in South Korea. *Water* **2018**, *10*, 765. [[CrossRef](#)]
47. Yue, S.; Wang, C. The mann-kendall test modified by effective sample size to detect trend in serially correlated hydrological series. *Water Resour. Manag.* **2004**, *18*, 201–218. [[CrossRef](#)]
48. Gocic, M.; Trajkovic, S. Analysis of changes in meteorological variables using mann-kendall and sen’s slope estimator statistical tests in Serbia. *Glob. Planet. Chang.* **2013**, *100*, 172–182. [[CrossRef](#)]
49. Blain, G.C. Removing the influence of the serial correlation on the mann-kendall test. *Revista Brasileira de Meteorologia* **2013**, *29*. [[CrossRef](#)]
50. Yue, S.; Pilon, P.; Phinney, B.; Cavadias, G. The influence of autocorrelation on the ability to detect trend in hydrological series. *Hydrol. Process.* **2002**, *16*, 1807–1829. [[CrossRef](#)]
51. Burn, D.H.; Elnur, M.A.H. Detection of hydrologic trends and variability. *J. Hydrol.* **2002**, *255*, 107–122. [[CrossRef](#)]
52. Yue, S.; Pilon, P.; Cavadias, G. Power of the mann-kendall and spearman’s rho tests for detecting monotonic trends in hydrological series. *J. Hydrol.* **2002**, *259*, 254–271. [[CrossRef](#)]

53. Gilbert, R.O. *Statistical Methods for Environmental Pollution Monitoring*; John Wiley & Sons: Hoboken, NJ, USA, 1987.
54. Theil, H. A rank-invariant method of linear and polynomial regression analysis. In *Henri Theil's Contributions to Economics and Econometrics*; Springer: Berlin, Germany, 1992; pp. 345–381.
55. Grell, G.A.; Dudhia, J.; Stauffer, D.R. A Description of the Fifth-Generation Penn State/Ncar Mesoscale Model (mm5). 1994. Available online: <http://danida.vnu.edu.vn/cpis/files/Books/MM5%20Discription%20-%201995.pdf> (accessed on 23 August 2018).
56. McKee, T.B.; Doesken, N.J.; Kleist, J. The relationship of drought frequency and duration to time scales. In *Proceedings of the 8th Conference on Applied Climatology, Anaheim, CA, USA, 17–22 January 1993*; American Meteorological Society: Boston, MA, USA, 1993; pp. 179–183.



© 2018 by the author. Licensee MDPI, Basel, Switzerland. This article is an open access article distributed under the terms and conditions of the Creative Commons Attribution (CC BY) license (<http://creativecommons.org/licenses/by/4.0/>).